Characterization of the diurnal cycle of maximum rainfall in tropical cyclones

Manuel F. Rios Gaona[a,*], Gabriele Villarini[a]

[a] IIHR - Hydroscience & Engineering, The University of Iowa, Iowa City, Iowa, USA.

Abstract

We analyze the diurnal cycle of maximum rainfall from ~300 TCs from March 2014 through February 2017, by cross-referencing the path of tropical cyclones (TCs) and high-resolution rainfall estimates from IMERG (Integrated Multi-satellitE Rainfall from GPM - Global Precipitation Measurement mission). IMERG is a gridded satellite product that offers high-resolution rainfall estimates at a spatiotemporal resolution of 0.1°×0.1° every 30 minutes, which are particularly suitable for these analyses.

Because of the nature of the data, we use circular statistics. Circular statistics allows us to account for the natural periodicity of a random variable such as the time of the day at which maximum rainfall from TCs occurs. We follow the non-parametric approach of Mixtures of Von Mises-Fisher distribution (MvMF), which enables an easy-to-interpret parameter identification of multimodal and anisotropic distributions of the TC-rainfall. We stratify our analysis by storm duration, maturity, and intensity, basin of origin, radial

[*] Corresponding author

Email address: manuelfelipe-riosgaona@uiowa.edu (Manuel F. Rios Gaona)

proximity to the center of the storm, and whether the storm is over the ocean or land.

In general, and across all scales, we find that there are mainly two cycles of maximum TC-rainfall: one diurnal cycle with peaks at ~10 and ~22h (local time), and one semi-diurnal cycle with peaks at ~2 and ~5h (local time). Although in a smaller proportion, the latter exhibits a weak afternoon alternative, i.e., ~14 and ~18h (local time).

Keywords: Tropical Cyclones, Diurnal Cycle, Rainfall, Circular Statistics, IMERG

1. Introduction

Tropical cyclones (TCs) are phenomena of paramount importance not only for the rain they produce but also for the havoc they unleash, both in coastal and inland areas (e.g. Czajkowski et al., 2017; Khouakhi et al., 2017). They are also considered the deadliest type of weather-related disasters, as the death toll from ~2,000 storms (from 1995 through 2015) amounts to ~242,000 fatalities (UNISDR and CRED, 2017) or 251,384 (roughly equivalent to 40% of the total casualties from weather-related disasters) from 1980 to 2000 according to (UNDP, 2004, p.37). For instance, in 2017 Hurricane Harvey brought almost 125,000m^3 of rain, spread over four U.S. states (Fritz and Samenow, 2017). Averaged over the Houston area, the lowest total precipitation in seven days brought by Hurricane Harvey was 700.2mm, which is more than double of any previous record (315.8mm for seven days of rainfall) between 1950-2016 (Risser and Wehner, 2017). Put into perspective, this amount of rainfall is the equivalent to the yearly average precipitation in Houston (Burian and Shepherd, 2005; Fritz and Samenow, 2017). Overall, Hurricane Harvey produced the largest rainfall ever recorded of any hurricane affecting the United States (e.g. Emanuel, 2017; NOAA-WPC, 2017; Samenow, 2017). The number of fatalities caused by this storm is reported to be ~80 people (e.g. Moravec, 2017; van

Oldenborgh et al., 2017).

The impact exerted by TCs comes from the high-wave storm surges, extreme winds, and floods and landslides associated with the torrential rains they produce (e.g. Mendelsohn et al., 2012; Peduzzi et al., 2012). Out of these three factors, we devote our attention to the characterization of heavy rainfall from TCs given its direct relation to flooding, which in the last two decades has affected ~2.3 billion people (UNISDR and CRED, 2017). This is equivalent to 56% of the people affected by weather-related disasters. Hence, the characterization of heavy rainfall from TCs provides essential information to assess and evaluate the impact from landfalling TCs, helping thus potential affected communities to be more resilient against such natural hazards. Several studies have focused on TC-rainfall characterization. For instance, (Prat and Nelson, 2016) studied the contribution of TCs to extreme daily rainfall, whereas (Prat and Nelson, 2013) established the contribution of TC-rainfall to the seasonal precipitation totals for the southeastern United States. (Jiang et al., 2008) analyzed the rainfall distribution from landfalling TCs in the north Atlantic basin. All of the above studies were based on about one decade of satellite data. (Lonfat et al., 2004; Rios Gaona et al., 2018) are global studies in which TC-rainfall is characterized and stratified by basin and intensity (among other features) also from global satellite data.

The focus of this work is to delve into the diurnal cycle of TC-rainfall maxima. The number of studies about the diurnal cycle of TC-rainfall have grown in recent years due to the widespread development and availability of satellite rainfall estimates. (Bowman and Fowler, 2015) carried out statistical analyses over 15 years of TMPA 3B42 (Tropical Rainfall Measurement Mission - TRMM Multisatellite Precipitation Analysis) and IBTrACS (International Best Track Archive for Climate Stewardship) data to investigate the diurnal cycle of TC-rainfall, which they see as one potential component of precipitation variability in these storms. (Wu et al., 2015) studied the diurnal variations of oceanic TC-rainfall in their inner core and outer rainbands. Their study was also based on 15 years (1998-2012) of TMPA 3B42 data (1401 TCs), and focused only on oceanic storms (i.e., beyond 300km from coastlines). (Leppert II and Cecil, 2016) used TRMM's Microwave Imager (TMI) and Precipitation Radar (PR) to study the diurnal cycle of 208 storms in the Atlantic basin during the period 1998-2011. They stratified their analyses by radii (from 100 to 1000km, every 100km), by intensity (wind speed larger than 34 kt, and 64 kt), and by height (2, 8, and 10km). More recently, (O’Neill et al., 2017) examined cloud-resolving TC simulations to understand the wavelike diurnal cycle responses on quasi-steady TCs. They found evidence of diurnal wave propagation in the upper troposphere in eddy-temperature fields. (Tang et al., 2017) studied the sensitivity of hurricane Secondary Eyewall Formation (SEF) to solar insolation. Through a numerical simulation, (Navarro et al., 2017) determined the impact of periodic diurnal heating on a balanced vortex, highlighting the importance of clouds. The introductions of (Bowman and Fowler, 2015; Leppert II and Cecil, 2016; O’Neill et al., 2017) provide extensive literature (and recounted details) on the diurnal cycle of oceanic precipitation (e.g. Frank, 1977; Hai-Long et al., 2013), of TC-rainfall (e.g. Jiang et al., 2011; Wu et al., 2015), and of cloud-tops changes (e.g. Browner et al., 1977; Dunion et al., 2014; Kossin, 2002). Studies on the diurnal cycle of TC-rainfall contribute to the characterization and understanding of TC-rainfall variability from the diurnal insolation cycle on TCs. Such a variation is key to improve storm intensity prediction, and TC modelling on global climate systems, for instance.

Our work advances the knowledge of the diurnal cycle of maximum TC-rainfall because we use high-resolution satellite data and circular statistics. IMERG (Integrated MultisatellitE Retrievals for GPM - Global Precipitation Measurement mission) is a follow-up on almost two decades on continuous rainfall monitoring at global scales from TRMM and its equivalent TMPA products (Huffman et al., 2007). IMERG is a gridded rainfall product with a spatiotemporal resolution of 0.1°×0.1° every 30 minutes (Hou et al., 2014). Rainfall monitoring at high resolution from space nowadays serves as a key tool to develop and enhance societal applications such as fresh water availability, flood forecasting, landslide warning, water-borne disease propagation, and storm-tracking (Kirschbaum and Patel, 2016; Stanley et al., 2017). The main advantage with regard to storm-tracking is that from global rainfall estimates such IMERG one can track the precipitation path of such large scale storms that often are difficult to even quantify from ground-based sensors like gauges and weather radars. The IBTrACS data set offers a detailed record of TC-tracks and maximum sustained windspeed (MSW) of all the TCs worldwide since 1842 (and up to March 2017). By combining these two data sets, we can obtain a detailed and accurate description of the spatiotemporal variability of rainfall from TCs. This allows us to study the diurnal cycle of maximum rainfall for all the TCs (259) worldwide in a span of 3 years (GPM launched its core satellite on February 2014).

In addition to high-resolution satellite data, we use circular statistics, which represents the appropriate statistical framework for analyses of this kind. In circular statistics the data under analysis is represented as points over a unit circle, which is the support for "circular" variables (Pewsey et al., 2013). In a circular space, all data is equally likely to be distributed over a segment equivalent to 2π. This abstraction has the unique advantage to account for the intrinsic periodicity of a circular and/or directional variables, such as time of the day at which rainfall occurs or the azimuthal direction of the maximum sustained windspeed of a hurricane, for instance. A basic example is that of the average of a random variable that took place at 01:00 and 23:00, for instance. A linear analysis will tell us that the average time of such a random variable is 12:00. Due to the proximity of 01:00 and 23:00 in a 24-h circular space, the circular analysis will yield an average time of 00:00, which is a more correct approximation of the true nature of the random variable under analysis.

Work on TC-rainfall via circular statistics has not been carried out so far. The common approach is to apply linear statistics to draw the cyclic patterns (e.g., Hu et al., 2017). Recent and related work on the implementation of circular analysis in hydrometeorological topics include those of (Dhakal et al., 2015; Masseran, 2015; Villarini, 2016). (Dhakal et al., 2015) developed a non-parametric (circular statistics) approach that optimizes the bandwidth(s) of a Von Mises distribution (Sec. 2). Their approach assessed the non-stationarity of 60 years of maximum daily precipitation at ten locations in the northeastern United States. (Masseran, 2015) used non-parametric circular statistics to better characterize the wind regime in the northern region of Borneo (Malaysia). From almost one year of hourly wind direction data (one station only), they found that the finite mixture of Von Mises–Fisher approach (Sec. 2) systematically outperforms the one based on non-negative trigonometric sums. From annual maximum instantaneous peak discharges (~7,500 gage stations with at least 30 years of data), (Villarini, 2016) applied circular statistics to study the seasonality of flooding across the continental United States. Other examples of developments and implementations of circular statistics in earth sciences (including mixtures of Von Mises–Fisher probability density functions - MvMF-PDFs) include those by (Lark et al., 2014; Oliveira et al., 2012). To the best of our knowledge, our work is the first of its kind that offers a comprehensive and quantitative characterization of the diurnal cycle of TC-rainfall maxima, analyzed via the circular statistics framework.

A detailed presentation of the theoretical framework of circular statistics is beyond the scope of this paper. For that matter, we point the interested reader to previous works carried out by (Fisher, 1993b; Mardia, 1972b; Mardia and Jupp, 2000; Pewsey et al., 2013), where deep and comprehensive formulations, details, and references on the theory of circular statistics can be found. Our approach relies on the **R**-packages **movMF** (Hornik and Grün, 2014), **circular** (Agostinelli and Lund, 2017), and **Directional** (Tsagris et al., 2017). **R** is computing language and environment for statistical analysis (R Core Team, 2017).

We stratify our analysis by TC duration, maturity, and intensity, basin of origin, distance from the center, and whether the storm is over the ocean or land. A thorough analysis of yet another characteristic of TC-rainfall such as the diurnal cycle of maximum TC-rainfall gets us closer to more realistic representations and models of the rainfall associated with TCs. We consider our approach a better assessment of the diurnal cycle because not only the available high-resolution data we use but also the circular framework offers a more accurate and appropriate approach for the statistical description of TC-rainfall maxima.

This paper is organized as follows: Section 2 briefly describes the data we use and introduces the conceptual framework of circular statistics, and its implementation. Section 3 presents the results and discussion alongside. Summary and conclusions are provided in Section 4.

2. Data and Methodology

Our data set is similar to that of (Rios Gaona et al., 2018), in which they analyzed 166 TCs for the period of March 2014 through March 2016. Hence, the analysis comes from the merging of two data sets: IBTrACS, and IMERG V04 Final.

The IBTrACS (v03r10) is a worldwide collection of TC best-track data (Knapp et al., 2010). Developed by the National Climatic Data Center (NCDC) jointly with the World Data Center for Meteorology, it is a comprehensive project that gathers information from all the Regional Specialized Meteorological Centers (RSMCs) and Tropical Cyclone Warning Centres (TCWCs) members of the World Meteorological Organization (WMO), and other national agencies (IBTrACS data is freely available from the server ftp://eclipse.ncdc.noaa.gov/pub/ibtracs/). The IBTrACS data set contains several attributes or variables. One of them is the seven basins in which the Earth's surface is divided into from a TC perspective: North Atlantic (NA), Eastern Pacific (EP), Western Pacific (WP), Northern Indian Ocean (NI), Southern Indian Ocean (SI), South Pacific (SP), and South Atlantic (SA). Attributes such as MSW, the time at landfall (if available), and the longitude and latitude of the storm centers (from which later we interpolate the TC track at 30-minute resolution) are also included in this data set. The temporal resolution of IBTrACS is 6 hourly (00:00, 06:00, 12:00, and 18:00 UTC).

IMERG is a gridded rainfall product (Level 3) from the GPM mission. This high-resolution product provides rainfall intensities with a spatiotemporal resolution of 0.1°×0.1° every 30 minutes between 60°N–60°S. It is obtained by processing (i.e., intercalibration, merging, and spatiotemporal interpolation) all the microwave precipitation estimates available from the GPM constellation (Huffman et al., 2017b). IMERG also incorporates infrared data from geostationary satellites, and it is calibrated with global gauge analyses of precipitation (Schneider et al., 2015a, 2015b). With three "flavors", IMERG products are developed to address different user requirements of latency and accuracy, i.e., Early Run (near-real-time), Late Run (reprocessed near-real-time), and Final Run (post-real-time). Technical insights on IMERG and its recent update IMERG V04 (Final) can be found in

(Huffman et al., 2017a, 2017b, 2017c). The availability of IMERG–Final goes from 12 March 2014 to the present with a latency of four months. This availability limits the number of TCs that one can potentially analyze. IMERG products contain several attributes (subsets). We only focus on the *precipitationCal* subset which offers the most accurate rainfall estimates. From here onwards, we refer to IMERG V04 Final (*precipitationCal*) only as IMERG. (GPM rainfall datasets are freely available at the NASA (National Aeronautics and Space Administration) portal http://pmm.nasa.gov/data-access/downloads/gpm).

Any circular variable (or observation) represented as a unit vector $\mathbf{x}$ is equivalent to complex number $z = e^{i\theta} = \cos\theta + i\sin\theta$, where $i = \sqrt{-1}$. Such a unit vector can be placed in the complex plane with its real component ($\cos\theta$) on the horizontal axis, and its imaginary component ($i\sin\theta$) on the vertical axis. For a graphic interpretation consult (Mardia and Jupp, 2000, Fig. 2.1; Pewsey et al., 2013, Fig. 3.1).

Summary statistics such as the sample mean direction ($\bar{\theta}$) and resultant length ($\bar{R}$), and circular variance (V) can be computed from circular data on the complex plane. The sample mean direction indicates the direction of the mean resultant (unit) vector of the sample (Pewsey et al., 2013, ch.3). It is given by $\bar{\theta} = \tan^{-1}(b/a) \in [0,2\pi)$, where $b = n^{-1}\sum_{j=1}^{n}\sin\theta_j$, and $a = \left[\sum_{j=1}^{n}\cos\theta_j\right]/n$ (only valid for $a \wedge b \neq 0$), θ_j represents the angle of a unit vector j with regard to the chosen zero/north, and n the sample size. As noted by (Pewsey et al., 2013, ch. 3), the sample mean direction is a good measure of central location for unimodal samples that are close to symmetric. The sample mean resultant length is defined by $\bar{R} = \sqrt{b^2 + a^2} \in [0,1]$, and it is used as a measure of “concentration” for unimodal circular data (Pewsey et al., 2013, ch.3). If all the unit vectors j are identical then $\bar{R} = 1$. Conversely, the more $\bar{R}$ approaches 0, the more evenly spread around the unit circle the data is. A particular case where $\bar{R} = 0$ may imply that all unit vectors cancel each other out, meaning that they all are evenly directed in the complex plane. The sample circular variance is defined as $V = 1 - \bar{R} \in [0,1]$. κ is the concentration parameter, equivalent to the "reliability" (σ^{-2}) of a normal distribution (Murray and Morgenstern, 2010). It can be obtained by linear interpolation from tabulated values of $\bar{R}$ (e.g., Mardia, 1972b, p.298, Table Appendix 2.3) or n and $\bar{R}$ (e.g., Mardia and Jupp, 2000, p.364, Table Appendix 2.5).

Several tests have been developed to evaluate or infer the uniformity and symmetry conditions of the sample. (Pewsey et al., 2013, ch. 5) strongly recommend the Rayleigh test for departure from uniformity in unimodal circular distributions. For multimodal departures from uniformity, they advise omnibus tests such as Kuiper's V_n, Watson's U^2, and Rao's spacing test, for instance. All the previous tests are for continuous circular data (i.e., data not grouped into bins). (Dhakal et al., 2015) noticed that while the Rayleigh is powerful against unimodal alternatives of uniformity (but not against multimodal alternatives, as suggested by (Pewsey et al., 2013)), the Rao's spacing and Kuiper's V_n tests are consistent against unimodal and multimodal alternatives of uniformity. A parametric bootstrap adaptation of the Watson's U^2 test is one alternative to test the goodness-of-fit of a specified distribution (Agostinelli and Lund, 2017; Tsagris et al., 2017). A sample can also be tested for two types of symmetry on the unit circle, reflective symmetry and ℓ-fold symmetry. A distribution is reflectively symmetric about an angle θ if the reflection of the distribution over such an angle is identical to the original distribution (Pewsey et al., 2013, ch.4). If a distribution is identical to the original distribution after being rotated through an angle $2\pi/\ell$, such a distribution is said to be ℓ-fold symmetric. For simplicity, we only test for reflective symmetry. A mathematical description of all these tests is beyond the scope of the present work. Still, we perform all of the above-mentioned tests (Sec. 3) to improve on the summary statistics, and gain a better perspective on the underlying distribution from which the sample is potentially drawn.

Our data exhibits multimodality (Fig. 1), therefore we follow the approach of a finite mixture of unimodal Von Mises–Fisher (MvMF) distributions. Non-parametric approaches (e.g., MvMF) offer more complex alternatives to account for the multimodality and asymmetry of irregular samples. The Von Mises distribution is a classic model in circular statistics, and it is considered the “equivalent” to the normal distribution model for linear data (Fisher, 1993b; Pewsey et al., 2013, ch. 4). It is also the most common, and more investigated approach given its easy-to-interpret parameters (Pewsey et al., 2013, ch. 4). The Cardiod, Wrapped Cauchy, Von Mises, Jones-Pewsey family, and Inverse Batschelet family models are alternative unimodal distributions developed to fit continuous circular data. For more details see (Pewsey et al., 2013, ch. 4).

As clearly presented and explained by (Qin et al., 2016) (see also Dhillon and Sra, 2003; Hornik and Grün, 2014), the D-variate Von Mises–Fisher distribution of a D-dimensional unit random vector $x\ \{\text{for } x \in \mathbb{R}^D, \text{in the unit hypersphere } \mathbb{S}^{D-1}, \text{and } \|x\| = 1\}$ follows the probability density function:

$$f(x|\mu,\kappa) = C_D(\kappa) \cdot \exp(\kappa \cdot \mu^T x). \tag{1}$$

In Eq. (1), $\kappa\ \{\text{for } \kappa \geq 0\}$ is the concentration parameter that quantifies how tightly the distribution is around the mean direction $\mu\ \{for\ \|\mu\| = 1\}$, $\mu^T x$ is the cosine similarity between x and μ, i.e., $\cos(x-\mu)\ \{\text{for } x \text{ and } \mu \text{ expressed in radians}\}$; and $C_D(\kappa)$ is a normalizing constant defined as:

$$C_D(\kappa) = \frac{\kappa^{D/2-1}}{(2\pi)^{D/2} \cdot I_{D/2-1}(\kappa)}, \text{where} \tag{2}$$

$$I_{D/2-1}(\kappa) := \sum_{s=0}^{\infty} \frac{1}{s! \cdot \Gamma(s + D/2 - 1 + 1)} \cdot \left(\frac{\kappa}{2}\right)^{2\cdot s + D/2 - 1}.$$

In Eq. (2), $I_{D/2-1}(\kappa)$ is the infinite series form (Arfken et al., 2013, Eq. (14.99)) of the modified Bessel function of the first kind with order $D/2 - 1$ and argument κ, and $\Gamma(s + D/2 - 1 + 1) := (s + D/2 - 1)!$ the gamma function. In our case, $D = 2$, and the D-variate Von Mises–Fisher distribution (Eq. (1)) reduces to the Von Mises distribution for the unit circle (Fisher, 1993a; Mardia, 1972a; Pewsey et al., 2013).

The simplest and most common approach in multimodal probability density functions for circular statistics is that of a finite mixture of Von Mises–Fisher (MvMF), which is given by, e.g., (Qin et al., 2016):

$$f\left(x \middle| \{\alpha, \mu, \kappa\}_{h=1}^{H}\right) = \sum_{h=1}^{H} \alpha_h \cdot f(x|\mu_h, \kappa_h), \text{for} \tag{3}$$

$$0 \leq \alpha_h \leq 1, \text{and} \sum \alpha_h = 1.$$

In Eq. (3), α_h is the mixing proportion of the H-unimodal Von Mises–Fisher distributions (PDFs). This equation has no analytical solution, hence its parameters are computed via Maximum Likelihood Estimates under an Expectation Maximization framework (Banerjee et al., 2005; Dhillon and Sra, 2003). The interested reader is pointed to the numerical solution implemented by (Hornik and Grün, 2014), given that is from the R-package **movMF** that we compute the parameters $(\alpha_h, \mu_h, \kappa_h)$ of the assumed MvMF–PDFs.

An objective assessment of the optimal/best mixture (number) of H-unimodal Von Mises–Fisher distributions is that of Akaike's or Bayesian information criterion (AIC or BIC, respectively, (Pewsey et al., 2013, p.114, ch.6)). The idea behind these criteria is to select the least complex of all models providing equally good fits (i.e., parsimony). We use the BIC criterion to select the number of distributions for a given MvMF–PDFs.

As with (Rios Gaona et al., 2018), we downscaled IBTrACS attributes to 30-minute IMERG native resolution. We interpolated the 6-hour TC-centers to 30-minute resolution via cubic spline interpolation of latitudes and longitudes. Hence, the interpolated TC-centers are not absolutely accurate. Nevertheless, the variability generated by such a method has no practical effect on the radii-averaged precipitation (Bowman and Fowler, 2015). For every 30-minute TC-center, we extracted IMERG rainfall up to a radius of 1,000km, every 7km from the TC center outwards (i.e., 0km, 7km, 14km ...). For each radius, we averaged all the rainfall depth from the TC center up to the radius under consideration. Following (Bowman and Fowler, 2015; Wu et al., 2015), we compute the local time (LST, T_{LST}) of all radii as the difference from their UTC (T_{UTC}) with regard to their longitude $\lambda \in [-180°, +180°]$, i.e., $T_{LST} = [T_{UTC} + \lambda(12/180)]$. For each storm we select the LSTs at which all maximum rainfall averages occur.

We stratify our analysis into six categories: storm duration, storm development, storm intensity, basin of origin, radial proximity to the TC center, and surface (land or ocean). The basin-of-origin and surface categories are entirely based on the coordinates of the TC center. A TC is considered to be over land if its center is geographically located over land, regardless of its proximity to the shore. We define three radial intervals to further stratify our analysis of maximum rainfall with regard to its proximity to the TC center. The storm-duration category is based on the day, relative to the storm beginning, from which a LST (or maximum TC-rainfall) was sampled, whereas the storm-development category is based on the quartile from which a given LST was sampled. The intensity-category is based on the MSW of the storm (for a given center). The MSW for a given 30-minute TC center corresponds to the previous 6-hourly step stored in the IBTrACS. We re-categorized the TC intensity into four categories based on the Saffir-Simpson Hurricane Scale (SSHS - Simpson, 1974): for MSW < 64 kt (33.1 $m \cdot s^{-1}$, TS), for 64 ≤ MSW < 96 kt (33.1 ≤ MSW < 49.4 $m \cdot s^{-1}$, CAT12), for MSW ≤ 96 kt (CAT35), and extra-tropical cyclones (ET).

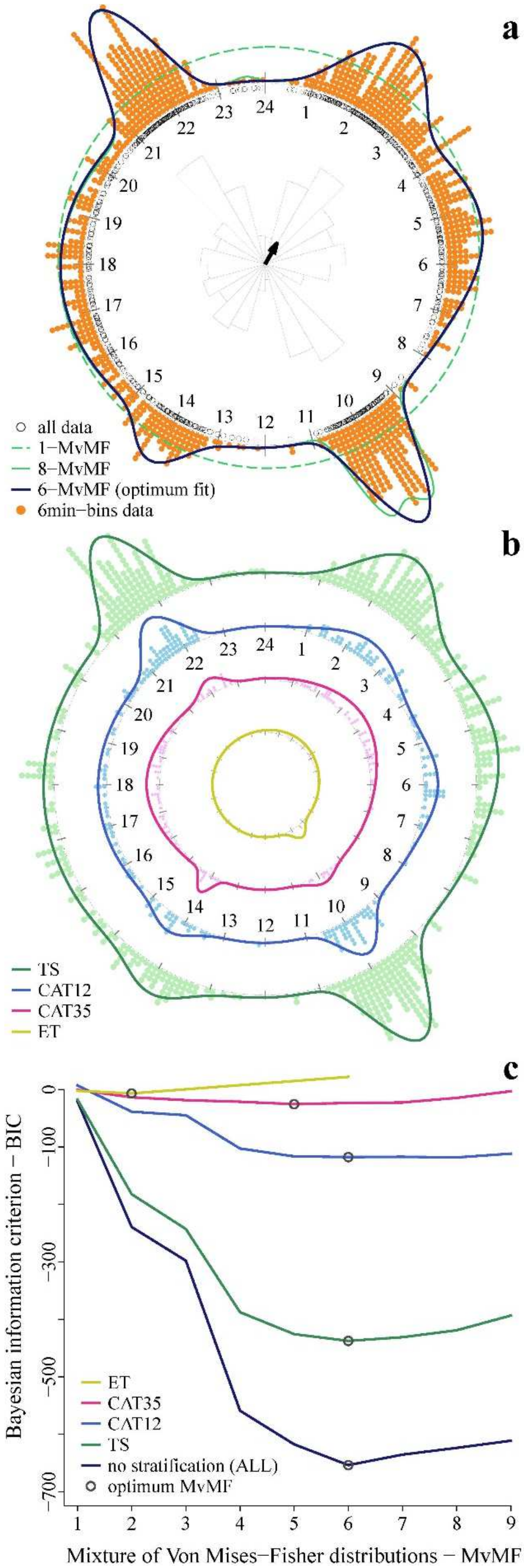
a
all data
1−MvMF
8−MvMF
6−MvMF (optimum fit)
6min−bins data
b
TS
CAT12
CAT35
ET
c
Bayesian information criterion − BIC
0
−100
−300
−500
−700
ET
CAT35
CAT12
TS
no stratification (ALL)
optimum MvMF
1
2
3
4
5
6
7
8
9
Mixture of Von Mises−Fisher distributions − MvMF

Figure 1: a. Circular distribution for 6-min-bins data (orange dots), and continuous data (black circles), for a 1024-value sample of maximum rainfall per storm. The dark blue continuous curve indicates the optimal MvMF-PDFs (6 mixtures), whereas the continuous green curve represents a fit of 8 mixtures, and the dashed green curve a fit of 1 vMF-PDF. The direction and magnitude of the black arrow are the sample mean direction ($\bar{\theta}$), and the sample mean resultant length ($\bar{R}$), respectively. A 1-h-bin circular histogram is also plotted. b. Circular distributions and best-fit MvMF-PDFs for TCs stratified by intensity, i.e., TS (green), CAT12 (blue), CAT35 (pink), and ET (gold). c. Bayesian information criterion (BIC) against a given number of MvMF, for the intensities in panel b, and the optimal mixture in panel a. (dark blue curve). The circles indicates the lowest point of the related BIC curve, which represents the optimal number of vMF mixtures that best describes the sample multimodality, i.e., 2 for ET, 5 for CAT35, and 6 for CAT12, TS, and all data (no stratification applied).

3. Results and Discussion

The summary statistics for the sample of 1024 unit vectors that represent the LSTs at which maximum precipitation (per storm for all the 259 TCs under analysis) occurs are: $\bar{\theta}$=1.952 hours or 0.5111 radians (sample mean direction), $\bar{R}$=0.131 (sample mean resultant length), and V=0.8693 (sample circular variance). The concentration parameter (κ) is 0.26375. Bear in mind that as the sample of average rainfall per TC is really large (multiple radii per several TC-centers), each storm can potentially have several rainfall estimates of equal maximum value (especially if one uses up to two significant figures/digits in the rounding up). This is why in this case we have a 1024-maximum sample for 259 TCs.

The p-value for the Rayleigh was 0, which indicates the rejection of the null hypothesis of uniformity. The p-values for the Kuiper's V_n, Watson's U^2, and Rao's spacing tests were smaller than 0.01, 0.01, and 0.001, respectively, which led us to the rejection of the null hypothesis of uniformity. The “goodness-of-fit” test for the grouped data as presented in Fig. 1-a, i.e., 6-min bins yielded p-values of 0.026, and 0.743 for the null hypotheses of uniform, and Von Mises distribution, respectively. Therefore, the null hypothesis of a uniform distribution that fits the sample is rejected (with a 2.6% significance level). The p-value for the reflective symmetry test was 0.053, which implies the rejection of the null hypothesis of an assumed reflectively symmetric distribution at the 5.3% significance level. The result of all these tests, jointly with a visual evaluation of Fig. 1-a, suggests that a-priori assumptions of isotropy, unimodality and reflective symmetry do not hold for our sample. Hence, we must turn to non-parametric circular statistics to evaluate and quantify the multimodality present in the diurnal cycle of maximum TC-rainfall (Fig. 1, for instance).

Fig. 1-a shows the distribution of the 1024 samples for TC-rainfall maxima, grouped into 6-min bins. In both distributions, either continuous or stacked, one can see how the data is not equally distributed over the circular space (anisotropy and multimodality). Maximum TC-rainfall tends to concentrate roughly around five times, i.e., ~2, 5, 10, 14, and ~22h; and somewhat spread between 15 and 21h (~18h average). This figure also highlights how summary statistics are misleading if some a-priori knowledge on the type-of distribution is not known. In Sec. 2, we established the MvMF distributions as the appropriate approach for a non-parametric multimodal fitting given its easy-to-interpret parameters. A visual inspection of Fig. 1-a reveals that, most likely, a mixture of 5 vMF-PDFs should be sufficient to describe well the sample distribution.

Fig. 1-c shows the BIC values for different number of unimodal vMF-PDFs (mixtures). Six is the optimal number of unimodal vMF-PDF for the overall distribution, i.e., no stratification implemented. As seen from Fig. 1-a, a single unimodal vMF-PDF is not suitable to identify the diurnal cycle. On the other hand, an 8-MvMF-PDF offers a quite detailed, and parametrized distribution at the expenses of parsimony. Nevertheless, Fig. 1-c tells us that only 6 vMF-PDFs are necessary to accurately account for the multimodality of the sample's distribution, and thus to identify the diurnal cycle of TC-rainfall. This can be seen from Fig. 1-a on how the continuous dark blue curve (6 vMF-PDFs) simply and accurately comprises the information gathered by the continuous green

curve (8 vMF-PDFs). Fig. 1-c also shows the BIC values for the stratification of TC-rainfall maxima given the intensity category (i.e., TS (green curve), CAT12 (blue curve), CAT35 (pink curve), and ET (gold curve)). The optimal mixture for each of these distributions is 6, 6, 5, and 2, respectively. This optimal fit can also be seen in Fig. 1-b, in which the MvMF-PDFs are plotted over the binned sample distribution of each intensity category.

Numerical solutions for small-size samples often yield large values of κ, which consequently yield infinite (∞) values of probability $f(x|\mu,\kappa)$ (Eq. (1)). Hence, the MvMF-PDFs here presented (e.g., Table 1) correspond to the lowest possible BIC obtained (from 1 to 9 components) for which all of its unimodal vMF-PDFs are finite and/or defined.

The four predominant mean times (μ's) of the diurnal cycle of TC-rainfall maxima are 2.22, 5.20, 9.88, and 21.75h (Fig. 1-a, and Table 1 - ALL rows). These times account for the largest κ's and α's, i.e., the concentration parameter and mixing proportion of each unimodal vMF-distribution, which describe ~72% of the MvMF-PDF of TC-rainfall maxima. About 22% of the distribution is described by the mean direction μ=17.80h, which is spread between ~15 and ~21h. This distribution has the lowest concentration parameter (κ=2.36), which is an indication of how sparse the sample is around its μ. The remaining ~6% belongs to μ=14.02h, with a high κ despite its lowest contribution to the MvMF-PDF. Hence, it seems that there are two main cycles of rainfall maxima in TCs: one with mean directions (μ) of 9.88 and 21.75h (note the ~12h of difference), referred to as the ~10–22h diurnal cycle; the other with mean directions of 2.22 and 5.20h, referred to as the ~2–5h (or ~22–2–5h) semi-diurnal cycle. This latter is also perceived, although very slightly, in the afternoon hours, i.e., ~14–18h (or ~10–14–18h) semi-diurnal cycle. (Navarro et al., 2017) showed a cycle in storm intensity that reaches its peak in the “early hours” of the morning, and lags a periodic response of ~6h from latent heat. Their results suggests that the axisymmetric TC diurnal cycle is primarily a balanced response driven by periodic heating. Such a signal is a function of the local solar time, which can helps to explain our similar results regardless of stratification by basin or type of surface. (Navarro et al., 2017) also hint at the extension of the cycles, arguing that long diurnal periods exhibit a more balanced solution with greater impact on the storm intensity, whereas short diurnal periods project onto inertia–buoyancy waves, radiating energy away from the region of heating.

The general (ALL) MvMF-PDF is quite representative of the samples over the ocean, as 97.4% of all TC-rainfall maxima correspond to TC-centers located over ocean. This can be seen from Fig. 2-f (ALL and Ocean curves) and from the very similar MvMF-PDF parameters in Table 1 - ALL and Ocean rows. For maximum TC-rainfall from TC-centers located inland, its mean direction is 2.06h with κ=0.45 (Table 1 - Land rows). Even though nothing conclusive can be inferred or concluded from such a small sample (~2.6% of data), it is widely known that TCs weaken as they move inland, which complicates the identification of a diurnal cycle for inland maximum TC-rainfall. (O'Neill et al., 2017) found that over land and on average, tropical rainfall rates reach their maximum in the afternoon. According to (Dai, 2001; Wu et al., 2015), convective precipitation over land tends to peak in the late afternoon to early evening hours (most likely to a direct response to daytime heating of the surface and the planetary boundary layer), whereas over oceans the peak is reached in the early morning hours. They did not explore ocean-land stratification though. On the other hand, (Bowman and Fowler, 2015) carried out an ocean-land, basin and intensity stratification. They suggested that either the TC-land interaction (landfall) has little incidence on the diurnal behavior of the storms, or that as storms move inland they retain their oceanic pattern/cycle until the land fraction is too large for this pattern to be present. More generally, (Bowman and Fowler, 2015) found a diurnal variation of TC-rainfall with peak rainfall at ~06:00 LST, and a minimum at ~18:00 LST. Although our results do show a lag of 12h for both diurnal and semi-diurnal cycles, our results do not show maxima at ~06:00 LST but rather at ~9.88h (LST) (or even at ~5.20h). Nevertheless, and as seen in Table 1 - ALL rows, several maxima are scattered around μ=17.80h. A different and larger sample (i.e., 15 years of TMPA-3B42 data), and an alternative approach (i.e., characterization of the diurnal cycle of rainfall in terms of Fourier harmonics by sines and cosines fitting via least squares regression), may be the reasons behind the discrepancy between our maxima (~9.88h) and the one (~06:00) of (Bowman and Fowler, 2015). Such diurnal cycles of oceanic precipitation with maxima in early morning hours (Bowman and Fowler, 2015) are common in studies such as (Gray and Jacobson Jr., 1977; Kraus, 1963; Serra and McPhaden, 2004), just to cite a few. (Jiang et al., 2011) also performed an ocean-land stratification in which they found two peaks for the diurnal variation of TC-rainfall over land: one at ~01:30–07:30 LST, and the other one at 16:30–19:30 LST (minimum at 10:30–13:30 LST). They also found maximum TC-rainfall at 04:30–07:30 LST (and minimum ~19:30–22:30 LST) for non-stratified analyses. As seen from Fig. 2-f and Table 1 - ALL rows, the maximum by (Jiang et al., 2011) is consistent with the second peak of the ~2–5h semi-diurnal cycle, i.e., μ=5.20±1h. With regard to our land stratification, our results showed an absence of any diurnal cycle (Table 1 - by SURFACE rows, and Fig. 2-f). Radial stratification, as suggested by (Bowman and Fowler, 2015), is an alternative to reduce the impact on the diurnal cycle amplitude of averaged TC-rainfall involving potentially non-raining areas (at large radii). Nevertheless, a sensitivity analysis carried out by (Wu et al., 2015) indicates that the decrease in average rainfall and diurnal variation in the outer rainbands is not attributable to such non-raining averages.

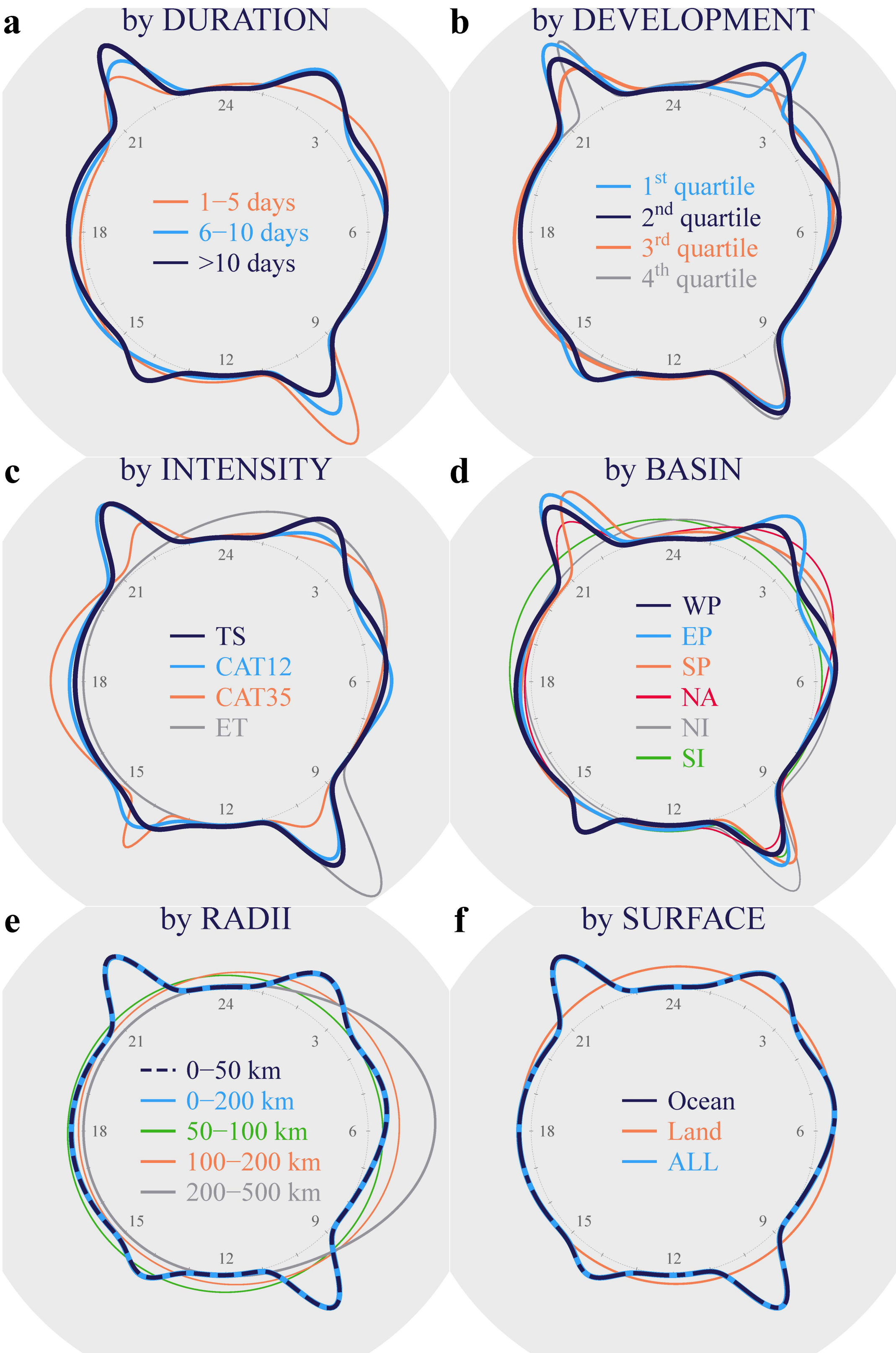

a
by DURATION
1–5 days
6–10 days
>10 days
b
by DEVELOPMENT
1st quartile
2nd quartile
3rd quartile
4th quartile
c
by INTENSITY
TS
CAT12
CAT35
ET
d
by BASIN
WP
EP
SP
NA
NI
SI
e
by RADII
0–50 km
0–200 km
50–100 km
100–200 km
200–500 km
f
by SURFACE
Ocean
Land
ALL
24
3
6
9
12
15
18
21

Figure 2: Mixtures of Von Mises-Fisher probability density functions (MvMF-PDFs) for stratifications by storm duration (a), storm development (b), storm intensity (c), basin of origin (d), radii proximity (e), and surface (f). The light-grey region indicates the maximum κ among all stratification, so individual concentration parameters among all MvMF-PDFs can be visually compared.

Short-living storms only develop a semi-diurnal cycle, whereas intermediate and long-lasting TCs develop stable diurnal and semi-diurnal cycles of maximum rainfall. A temporal stratification of maximum TC-rainfall with regard to the number of days a given TC lasts shows that for short-living TCs, namely TCs that last up to five days, there is mainly a ~10–22h diurnal cycle (Fig. 2-a). Its μ's are clustered around 9.90 and 21.52h, with κ's of 98.15 and 65.51, respectively (Table 1 - by DURATION rows). Fig. 2-a also shows a ~10–14h semi-diurnal cycle (μ=14.01 with κ=73.61) for long-lasting storms, and a much less marked one (κ=3.47) for short-living storms. As we show later, this ~10–14h semi-diurnal cycle is mainly characteristic of TCs developed in the WP basin (Fig. 2-d). Intermediate and long-lasting storms (i.e., TCs lasting more than 10 days) follow a similar dynamic in terms of both diurnal and semi-diurnal cycles. Their ~10–22h diurnal cycles show μ's of 9.89 and 9.87h, and 21.77 and 21.76h, respectively for intermediate and long-lasting TCs. As the storm lasts longer (e.g., more than 10 days), maximum TC-rainfall seems to be more concentrated at the end of the diurnal cycle than at its beginning. This can be seen from the larger values of κ, i.e., 60.14 and 116.60 at ~22h than those of 108.12 and 67.88 at ~10h (Table 1 - by DURATION rows, and Fig. 2-a). Intermediate and long-lasting TCs have similar ~22–2–5h semi-diurnal cycles (i.e., μ's of 2.20 and 5.74h for intermediate TCs, and μ's of 2.23 and 4.97h for long-lasting TCs).

A second temporal stratification showed that as the storms reach their end, maximum TC-rainfall develops earlier in the day (rather than later). When the duration of all TCs were stratified into quartiles, the first quartile (i.e., the first 25% of any storm, Fig. 2-b – light blue curve, and Supplemental Fig. 2 - q1) distinctively showed one diurnal ~10–22h cycle

(μ's of 9.86 and 21.72h), and two semi-diurnal cycles, which are distinctively marked around the μ's of 2.42 and 14.15h. The ~5h (or ~17h) component of the semi-diurnal cycle does not fully develop for this quartile (Supplemental Fig. 2 - q1). Bear in mind that ~22- and ~2-h μ's are only characteristic of intermediate and long-lasting storms (Fig. 2-a). The κ's for this first quartile are larger for ~22–2h (i.e., 92.50, and 511.50) than for ~10–14h (i.e., 76.98, and 40.06). This implies a larger concentration of maximum TC-rainfall during "night" (~22–2–5h semi-diurnal cycle) than "day" hours (~10–14–18h semi-diurnal cycle). As the storms develop, i.e., 2nd and 3rd quartiles, the larger concentration of maximum TC-rainfall shifts from ~22 to ~10h. Fig. 2-b (or Supplemental Fig. 2 - q2 or - q3) shows how the μ's for the 2nd and 3rd quartiles (i.e., 9.90 and 9.87h, respectively) present larger κ's (85.41 and 96.25) than those for the μ's of 21.66 and 21.83h (κ's of 91.63 and 51.08, respectively for the 2nd and 3rd quartiles). It appears that the ~2–5h semi-diurnal cycle is mostly characteristic of the 2nd and 3rd quartiles; stronger for the 2nd quartile, and weakening for the 3rd one, with more samples concentrated at ~2 than at ~5h (Table 1 - by DEVELOPMENT rows; and Supplemental Fig. 2 - q2 and - q3). The ~10–14h semi-diurnal cycle is not present anymore in the 3rd and 4th quartiles. The absence of multimodality for the last (4th) quartile, given also the extension of the sample, indicates that as the storm vanishes, no diurnal or semi-diurnal cycle of maximum TC rainfall can be identified (Supplemental Fig. 2 - q4). Our results for this alternative temporal stratification agree with the suggestion by (Navarro et al., 2017) that the magnitude of the diurnal signal may vary throughout the lifetime of the storm. According to them, results in the literature are mixed about the impact of TC diurnal cycle with regard to storm maturity, i.e., some advocate for impacts in the developing (early) stages (e.g., Hobgood, 1986; Melhauser and Zhang, 2014; Sundqvist, 1970), while others for impacts in the mature (late) stages (e.g., Craig, 1996; Tang and Zhang, 2016; Tuleya and Kurihara, 1981). Our results lay in both groups as the 2nd and 3rd (and even the 1st) quartiles show diurnal and semi-diurnal cycles.

The stratification by intensity shows that the overall (unstratified) MvMF-PDF is roughly based on the TS category. This can be seen from Fig. 1-b and Fig. 2-c, and the similar parameters in Table 1 - TS and ALL rows. For the TS category, the diurnal (~10–22h) and semi-diurnal (~2–5h) cycles of maximum TC-rainfall are equally distinctive. This can be seen from its κ's of 36.88, 9.31, 85.00, and 87.92, respectively for μ's of 2.23, 5.30, 9.89, and 21.72h. All of the above four vMF unimodal distributions account for ~75% of the mixture (~20% is described by μ=17.54h, with κ=1.65 the lowest for any category of intensity). TS is the only category with a weak ~10–14h semi-diurnal cycle around μ=13.90h. As with the stratification by surface, this behavior is expected for the TS category, which accounts for 61.1% of the maximum rainfall analyzed. CAT12 and CAT35 account for 24.7% and 13.1% of the sample, respectively. The MvMF-PDF for CAT12 is mainly described by a strong ~10–22h diurnal cycle with μ's of 9.89 and 21.65h (Table 1 - CAT12 rows). This strong diurnal cycle is responsible for ~39% of the distribution. About 33% of this MvMF-PDF comes from the less marked ~2–5h semi-diurnal cycle with μ's of 2.46 and 5.98h. Given that the largest proportion of the MvMF-PDF for CAT35 (~74%) comes from very diffused (κ's of 5.87 and 6.31) mean directions (μ's of 3.57 and 18.04h, respectively), we can ascertain the absence of any (semi-) diurnal cycle for extremely intense TCs. One of the causes for this absence might be related to the random nature of such an extreme maximum rainfall. This is yet to be proven, as there are few CAT35 samples (13.1%). Still, our results for CAT35 are in line with (Leppert II and Cecil, 2016) who associated intense TCs with a weaker diurnal signal. They based this assertion on studies such as (Browner et al., 1977; Hobgood, 1986). With only 1.1% of ET storms, no conclusive non-parametric analysis was possible for the ET category. Similar to (Bowman and Fowler, 2015), (Wu et al., 2015) stratified oceanic TC-rainfall (inner core, i.e., 0-100km, and outer rainbands, i.e., 100-500km) by weak (CAT1 and TS), and strong (CAT2-5) storms. (Wu et al., 2015) found that the daily maximum is reached at 02:30–05:00 UTC (inner core), and at 05:00–08:00 UTC (rainbands) for weak storms, whereas for strong storms these periods are 01:30–04:00 UTC (inner core) and 04:00–12:00 UTC (rainbands). In our case, all intensity categories encompass the early periods for either the inner core or rainbands, i.e., ~2.7±0.9h and ~5.6±0.4h, even though the early-hours shifting is not as large as the one in (Wu et al., 2015). Nevertheless, our analysis does not show correspondence with their late periods. With regard to inner core or rainbands, we later show that these periods remain “the same” for 0-200km (or 0-50km).

With regard to the stratification by basin, the two main diurnal cycles of maximum TC-rainfall are provided by the Pacific basin with 75.3% of the sample. The sample percentages for the SP, EP, WP, SI, NI, and NA basins are 15.4, 21.2, 38.7, 8.5, 8.1, and 8.1%, respectively. With μ's of 2.33, 5.36, 9.91, and 21.60h, the WP basin follows the ~10–22h diurnal and ~2–5h semi-diurnal cycles (Fig. 2-d – dark blue curve). It is also the only basin with a distinctive μ=14.12h, which suggests a late and light ~10–14–18h semi-diurnal cycle. For detailed κ values see Table 1 - by BASIN rows. WP is the basin that resembles the overall (ALL) MvMF-PDF the most (Fig. 2-f - light blue curve, and Fig. 1-a - continuous dark blue curve). This is probably due to its highest percentage of sampled TCs (38.7%). (Jiang et al., 2011) also found that the WP basin has the largest number of deepest and most intense tropical cyclone precipitation, cloud, and convective cell features. The EP and SP basins follow a pattern similar to the WP basin. Both present a distinctive ~10–22h cycle, and a less marked ~2–5h semi-diurnal cycle, practically absent in the SP basin. As seen from Supplemental Fig. 1, it appears that the ~2–5h semi-diurnal cycle is something really characteristic of the north Pacific basin (i.e., WP and EP basins; see also Table 1 - by BASIN rows). The non-parametric analysis is less conclusive for the SI, NI, and NA basins, which add the remaining quarter (24.7%) of the sample altogether. The Indian basin (SI and NI) presents a distinctive mean time ~10h, with κ's of 123.52 and 113.71, respectively for SI and NI. The difference between the SI and NI basins is that the latter shows a scattered sample (κ=0.83) at μ=2.77h, whereas the scattered sample for the former is at μ=20.66h (κ=0.80). Note the discordance of these μ's from the diurnal or semi-diurnal cycles. Such a disagreement may be influenced by non-parametric analyses based on few samples (8.3% on average for each Indian basin). The NA basin (Fig. 2-d - red curve, and Supplemental Fig. 1 - NA) has also one of the lowest samples (8.1%), which does not allow a clear identification of any diurnal cycle.

When the analysis was stratified by radii, the general pattern (ALL) mimicked that of the maximum TC-rainfall within 200km radii (Fig. 2-e – light blue curve). Thus, the ~10–22h diurnal cycle, and the ~2–5h and ~14–18h semi-diurnal cycles are mainly present within 200km from the TC-center (μ's of 2.22, 5.19, 9.88, 14.02, and 21.75h). For radii between 200 and 500km, there is only a weak (κ=3.33) μ=5.73h. This, and the fact that no maximum TC-rainfall was beyond 500km radii suggest that TC-maximum rainfall only develops within 200km radii. We stratify radii further down to three more intervals within 200km, i.e., 0-50, 50-100 (not presented here), and 100-200km. As shown in Table 1 (by RADII rows) and Fig. 2-e, 50km is descriptive of the overall behavior for maximum TC-rainfall within 200km, as these two radii (0-50 and 0-200km) follow almost identical diurnal and semi-diurnal cycles. Almost the entire sample (98.2%) is in the 0-50km range, whereas 99.7% is within 200km. (Wu et al., 2015) suggested that the outward propagation of the diurnal signals is associated with the internal structure of TC convective systems, regardless of the basins where they develop. Recent work presented by (Leppert II and Cecil, 2016) is somewhat in agreement with our results for radial stratification. They found that for 100-500-km radii TC-rainfall (clouds) peaks in the morning (01:30–07:30 LST), and that the minimum is reached between 10:30–19:30 LST. From Fig. 2-e, one can see the similarities of these peaks with the ~2–5h semi-diurnal cycle for radii shorter than 500km (or even 200km). Nevertheless, in what they call “minimum”, we have the ~10–22h diurnal cycle. Our ~22–2–5h semi-diurnal cycle also appears in their inner core (0-100km, “with a maximum at 22:30–04:30 LST”) associated with only upper levels (8-10km). According to (Leppert II and Cecil, 2016), the peak between 01:30–07:30 LST is also found in several previous studies (e.g., Bowman and Fowler, 2015; Lajoie and Butterworth, 1984; Muramatsu, 1983).

The MvMF-PDFs in Fig. 2-e represent PDFs of maximum TC-rainfall for several radii. As presented in (Rios Gaona et al., 2018), the average maximum TC-rainfall for the intervals 0-200km, 200-500km, and 500-1000km are 48.07, 11.61, and 3.41mm, respectively. Likewise, the average maximum TC-rainfall for the intervals 0-50km, 50-100km, and 100-200km are 48.04, 27.87, and 19.26mm, respectively. About 48mm of rainfall either for 0-50 or 0-200km confirms the vast representativeness of TC-rainfall maxima just within the first 50km from the TC-center. Such detailed statistics close to the TC-centers are possible thanks to the high resolution rainfall retrievals offered by IMERG.

Table 1: Mean times μ, concentration parameters κ; and mixing proportions α for up-to 6 MvMF-PDFs for un- and stratified TC-rainfall maxima. All the curves shown in Fig. 2 can be reconstructed if the parameters presented in this table are plug into Eqs. (3), (2), and (1). The 'size' is the percentage of a given category relative to its stratification.

MvMF-PDFs		#1	#2	#3	#4	#5	#6	size [%]
ALL (no stratification)								
	μ	2.2152418	5.2016072	9.8812249	14.0237249	17.8024248	21.7446129	
	κ	31.98304	8.89786	82.76682	68.67366	2.35992	82.38932	100
	α	0.1818	0.1798	0.1795	0.0632	0.2218	0.1739	
by DURATION								
1-5 days	μ	3.8888570	-	9.9019170	14.4064328	-	21.5235256	
	κ	3.91834	-	98.14502	3.46633	-	65.50892	15.8
	α	0.3931	-	0.2657	0.1873	-	0.1538	
6-10 days	μ	2.1977949	5.7379428	9.8905352	-	16.4961242	21.7734378	
	κ	31.34776	8.99902	108.11746	-	2.73278	60.13451	44.7
	α	0.2141	0.1548	0.1700	-	0.2669	0.1942	
>10 days	μ	2.2267869	4.9729403	9.8672777	14.0073784	18.1866170	21.7614043	
	κ	33.72356	9.92566	67.87566	73.60951	3.11870	116.60151	39.5
	α	0.1852	0.1771	0.1475	0.0714	0.2376	0.1813	
by DEVELOPMENT								
1st quartile	μ	2.4184217	4.0470154	9.8587574	14.1444514	17.3995804	21.7164537	
	κ	511.49821	3.30833	76.98216	40.05593	4.72186	92.49673	32.7
	α	0.0734	0.2841	0.1804	0.1028	0.1403	0.2191	
2nd quartile	μ	2.1408816	5.4999594	9.8999525	14.0022682	17.8312735	21.6622133	
	κ	33.17070	15.49447	85.40689	75.88738	2.82371	91.63058	31.8
	α	0.2314	0.1624	0.1894	0.0669	0.1775	0.1724	
3rd quartile	μ	1.9331084	4.6909351	9.8675160	-	16.9885625	21.8251026	
	κ	44.60595	6.55601	96.25009	-	2.26269	51.07975	29.2
	α	0.1217	0.2206	0.1602	-	0.3325	0.1650	
4th quartile	μ	-	3.6825855	10.0059731	-	16.6991725	21.9284509	
	κ	-	4.54927	99.61211	-	2.56488	283.27545	6.3
	α	-	0.4831	0.1827	-	0.2154	0.1188	
by RADII								
0-50 km	μ	2.1983336	5.1768204	9.8823541	14.0114995	17.7677399	21.7395741	
	κ	32.71734	9.12278	83.12776	67.38022	2.45511	82.79723	98.2
	α	0.1815	0.1780	0.1802	0.0623	0.2215	0.1765	
0-200 km	μ	2.2158813	5.1849830	9.8802406	14.0236901	17.8014777	21.7446034	
	κ	31.67820	9.23182	82.30998	68.71572	2.35887	82.38592	99.7
	α	0.1821	0.1774	0.1802	0.0634	0.2225	0.1744	
100-200 km	μ	-	-	-	12.8738133	-	-	
	κ	-	-	-	0.18349	-	-	0.5
	α	-	-	-	1.0	-	-	
200-500 km	μ	-	5.7290486	-	-	-	-	
	κ	-	3.33307	-	-	-	-	0.3
	α	-	1.0	-	-	-	-	

MvMF-PDFs		#1	#2	#3	#4	#5	#6	size [%]
by INTENSITY								
	μ	2.2271917	5.2946123	9.8851433	13.9043633	17.5407806	21.7197800	
TS	κ	36.88254	9.31251	85.00220	59.11905	1.65370	87.92400	61.1
	α	0.1984	0.1647	0.1985	0.0606	0.1923	0.1854	
	μ	2.4581381	5.9759664	9.8883872	14.2248417	17.7298958	21.6490429	
CAT12	κ	19.95348	19.52417	87.33768	66.70176	3.47275	74.19870	24.7
	α	0.1891	0.1381	0.1772	0.0794	0.2063	0.2099	
	μ	3.5711101	-	9.9043271	14.0923809	18.0361222	22.1192259	
CAT35	κ	5.87049	-	71.11366	266.51113	6.30509	79.32346	13.1
	α	0.3973	-	0.0742	0.0777	0.3469	0.1039	
	μ	2.5263721	-	9.6360580	-	-	-	
ET	κ	3.26545	-	71.66865	-	-	-	1.1
	α	0.6397	-	0.3603	-	-	-	
by BASIN								
	μ	3.7529389	-	9.7617842	15.9540656	-	22.0136527	
SP	κ	3.90692	-	110.68994	3.46186	-	96.25777	15.4
	α	0.4128	-	0.1787	0.2142	-	0.1943	
	μ	-	-	9.8441757	-	-	20.6582418	
SI	κ	-	-	123.52417	-	-	0.79691	8.5
	α	-	-	0.1347	-	-	0.8653	
	μ	2.3264704	5.3600035	9.9105106	14.1227946	17.2293971	21.6014794	
WP	κ	34.66562	9.89724	78.75968	137.32522	3.78443	94.58224	38.7
	α	0.1839	0.1775	0.1683	0.0622	0.2231	0.1850	
	μ	2.7692542	-	9.9647873	-	-	-	
NI	κ	0.83253	-	113.70709	-	-	-	8.1
	α	0.7786	-	0.2214	-	-	-	
	μ	2.4953669	5.8594334	9.9006361	-	16.5093351	21.6812694	
EP	κ	40.66527	32.67055	117.70027	-	1.42725	89.48307	21.2
	α	0.2445	0.0713	0.1646	-	0.3035	0.2161	
	μ	3.2040271	-	9.9497323	15.1860953	-	21.6652349	
NA	κ	5.83075	-	52.51851	1.80111	-	63.59554	8.1
	α	0.4628	-	0.1672	0.2139	-	0.1561	
by SURFACE								
	μ	2.2491078	5.2375259	9.8708787	14.0332012	17.7416074	21.7369835	
Ocean	κ	31.40649	9.78592	82.29653	66.17639	2.37856	81.33687	97.4
	α	0.1845	0.1739	0.1808	0.0647	0.2176	0.1785	
	μ	2.0573905	-	-	-	-	-	
Land	κ	0.45273	-	-	-	-	-	2.6
	α	1.0	-	-	-	-	-	

4. Summary and Conclusions

The goal of this work was to quantitatively assess the diurnal cycle of maximum TC-rainfall by means of non-parametric circular statistics. To do so, we cross-referenced the IBTrACS (v03r10) and IMERG (V04) data sets to accurately account for high-resolution rainfall within a 2,000km-wide swath along the path of a given TC. We analyzed 259 TCs that occurred from March 2014 through February 2017 (~3 years of data). The IMERG data set is a gridded satellite product of high spatiotemporal rainfall estimates (0.1°×0.1° every 30 minutes), which makes it very suitable for analyses related to the diurnal cycle of TC rainfall. Circular statistics is a mathematical framework that allows statistical analyses accounting for the intrinsic periodicity of circular/directional variables. In our case, such a circular (random) variable is the time of the day for which a TC-rainfall maximum occurred. We modelled the multimodality and anisotropy of TC-rainfall maxima using the finite mixtures (aggregations) of unimodal Von Mises-Fisher distributions (MvMF-PDFs), which is the most common approach, given its easy-to-interpret parameters (e.g., mean direction/time μ, concentration parameter κ, and mixing proportion α). We stratified our analysis by storm duration, maturity, and intensity, basin of origin, proximity of the TC-rainfall maxima to the storm center (i.e., by radii), and whether the TC center was over the ocean or land.

On average, when no stratification is implemented over the 259 TCs here analyzed, there are two main cycles of maximum rainfall: one with mean directions (μ) of 9.88 and 21.75h (κ's of 82.77 and 82.39, respectively), referred as the ~10–22h diurnal cycle; the other one with μ's of 2.22 and 5.20h (κ's of 31.98 and 8.90, respectively), referred as the ~2–5h semi-diurnal cycle. This semi-diurnal cycle appears to be also present at afternoon hours, i.e., ~14–18h (μ's of 14.02 and 17.80h with respective κ's of 68.67 and 2.36).

Ocean, TS (tropical storms, i.e., MSW < 64kt), WP (West Pacific), 0-200km (or even 0-50km) radii, long-lasting (i.e., storms with duration longer than 10 days), and 2nd quartile are the stratifications that resemble the general MvMF-PDF of the ~10–22, and ~2–5h cycles the most. All of these particular stratifications average μ's of 2.23, 5.26, 9.89, and 21.70h, with standard deviations of 0.061, 0.178, 0.017, and 0.060, respectively. This correspondence is mainly attributed to the large influence each of these stratifications exert on the sample. That is, out of the sample of 2014 values (of maximum TC-rainfall per storm), 97.4% comes from Ocean, 61.1% from TS, 38.7% from WP, 98.2% from radii smaller than 50km, 39.5% from storms lasting more than 10 days, and 31.8% from all their 2nd quartiles.

Short-lived TCs (i.e., 1-5 days) mainly develop a diurnal cycle (of maximum rainfall) around μ's of 9.90 and 21.52h (i.e., ~10–22h diurnal cycle). Intermediate, and long-lasting (i.e., 5-10 days, and longer than 10 days, respectively) TCs develop both diurnal (~10–22h) and semi-diurnal (~2–5h) cycles. Long-lasting storms show a weak ~14–18h semi-diurnal at μ=14.01h, which is mainly characteristic of TCs from the WP basin. As storms last longer, the maximum TC-rainfall distribution concentrates more at the end of the diurnal cycle (~22h) than at its beginning (~10h).

At an earlier stage of a storm (1st quartile) there is also a larger concentration of maximum TC-rainfall at the end of the diurnal cycle (μ=21.72h) than at its beginning (μ=9.86h). This concentration shifts towards the beginning of the ~10–22h diurnal cycle as the storm progresses to its 2nd and 3rd quartiles. The ~22–2–5h semi-diurnal cycle is mainly characteristic of the 2nd (μ's of 2.14 and 5.50h) and 3rd (μ's of 1.93 and 4.69h) quartiles. As the storm matures this semi-diurnal cycle weakens. No particular diurnal or semi-diurnal cycle is developed at the end of the storm (4th quartile).

While CAT12 storms show a distinctive ~10–22h diurnal cycle (μ's of 9.89 and 21.65h), CAT35 storms show an absence of any (semi-) diurnal cycles, which might be attributed to the very random nature of such an extreme maximum rainfall. It is reminded that CAT12 and CAT35 respectively account for 24.7 and 13.1% of the sample, and that nothing conclusive can be said for ET storms as only few samples of TC-rainfall maxima were within this category (1.1%).

All the Pacific basins (i.e., WP, EP - East Pacific, and SP - South Pacific) show a distinctive ~10–22h diurnal cycle. On average, their μ's are at 9.86 and 21.77h, with WP the basin with the larger number of samples (38.7% of TC-rainfall maxima). WP is the only basin with two distinctive semi-diurnal cycles, i.e., ~2–5h (with μ's of 2.33 and 5.36h), and ~14–18h (with μ's of 14.12 and 17.23h).

Neither the North Atlantic (NA) nor the Indian basins (SI - South Indian, and NI - North Indian) showed any distinctive diurnal and/or semi-diurnal cycles. Nevertheless, it appears that both Indian basins have predominant μ's ~9.91h, with a tendency for the SI basin to distribute maximum rainfall at μ=20.66h, and at μ=2.77h for the NI basin. These different values of μ's can be attributed to the lower number of samples the non-parametric analysis was based on (e.g., NA, NI and SI represent just 24.7% of the sample).

When the analysis was stratified by radii, the ~10–22h diurnal and ~2–5h semi-diurnal cycles are rather similar among the 0-50 and 0-200km radii, given that 99.7% of the sample is within 200km, and 98.2% within 50km radii. This is a clear indication that the diurnal cycle of maximum TC-rainfall takes place within the first 50km from the TC-center (outwards). No maximum TC-rainfall was found for radii beyond 300km.

The level of detail reached in this work was possible due to high- resolution and quality data sets such as IBTrACS and IMERG. Despite their intrinsic and potential deficiencies, the combination of such data sets offers a comprehensive record and a rather accurate evaluation of TC-rainfall. An accurate description (or modelling) of the diurnal cycle of maximum rainfall from TCs further propels better and more accurate TC-rainfall models, which in the end serves to increase our resilience against this type of natural hazards and their catastrophic consequences.

Acknowledgements

This material is based in part upon work supported by the National Science Foundation under CAREER Grant AGS-1349827, and Award NA14OAR4830101 from the National Oceanic and Atmospheric Administration, U.S. Department of Commerce.

References

Agostinelli, C. and Lund, U.: {R} package \texttt{circular}: Circular Statistics (version 0.4-93), [online] Available from: https://r-forge.r-project.org/projects/circular/, 2017.

Arfken, G. B., Weber, H. J. and Harris, F. E.: Chapter 14 - Bessel Functions, in Mathematical Methods for Physicists (Seventh Edition), edited by G. B. Arfken, H. J. Weber, and F. E. Harris, pp. 643–713, Academic Press, Boston., 2013.

Banerjee, A., Dhillon, I. S., Ghosh, J. and Sra, S.: Clustering on the Unit Hypersphere Using Von Mises-Fisher Distributions, J. Mach. Learn. Res., 6, 1345–1382 [online] Available from: http://www.jmlr.org/papers/volume6/banerjee05a/banerjee05a.pdf, 2005.

Bowman, K. P. and Fowler, M. D.: The Diurnal Cycle of Precipitation in Tropical Cyclones, J. Clim., 28(13), 5325–5334, doi:10.1175/JCLI-D-14-00804.1, 2015.

Browner, S. P., Woodley, W. L. and Griffith, C. G.: Diurnal Oscillation of the Area of Cloudiness Associated with Tropical Storms, Mon. Weather Rev., 105(7), 856–864, doi:10.1175/1520-0493(1977)105<0856:DOOTAO>2.0.CO;2, 1977.

Burian, S. J. and Shepherd, J. M.: Effect of urbanization on the diurnal rainfall pattern in {H}ouston, Hydrol. Process., 19(5), 1089–1103, doi:10.1002/hyp.5647, 2005.

Craig, G. C.: Numerical experiments on radiation and tropical cyclones, Quart. J. Roy. Meteor. Soc., 122(530), 415–422, doi:10.1002/qj.49712253006, 1996.

Czajkowski, J., Villarini, G., Montgomery, M., Michel-Kerjan, E. and Goska, R.: Assessing Current and Future Freshwater Flood Risk from North Atlantic Tropical Cyclones via Insurance Claims, , 7(art. no. 41609), doi:10.1038/srep41609, 2017.

Dai, A.: Global Precipitation and Thunderstorm Frequencies. Part II: Diurnal Variations, J. Clim., 14(6), 1112–1128, doi:10.1175/1520-0442(2001)014<1112:GPATFP>2.0.CO;2, 2001.

Dhakal, N., Jain, S., Gray, A., Dandy, M. and Stancioff, E.: Nonstationarity in seasonality of extreme precipitation: A nonparametric circular statistical approach and its application, Water Resour. Res., 51(6), 4499–4515, doi:10.1002/2014WR016399, 2015.

Dhillon, I. S. and Sra, S.: Modeling data using Directional Distributions. [online] Available from: http://www.cs.utexas.edu/users/inderjit/public_papers/tr03-06.pdf, 2003.

Dunion, J. P., Thorncroft, C. D. and Velden, C. S.: The Tropical Cyclone Diurnal Cycle of Mature Hurricanes, Mon. Weather Rev., 142(10), 3900–3919, doi:10.1175/MWR-D-13-00191.1, 2014.

Emanuel, K.: Assessing the present and future probability of Hurricane Harvey's rainfall, Proc. Natl. Acad. Sci., 114(48), 12681–12684, doi:10.1073/pnas.1716222114, 2017.

Fisher, N. I.: Models, in Statistical Analysis of Circular Data, pp. 39–58, Cambridge University Press., 1993a.

Fisher, N. I.: Statistical Analysis of Circular Data, Cambridge University Press, Cambridge, Great Britain., 1993b.

Frank, W. M.: The Structure and Energetics of the Tropical Cyclone I. Storm Structure, Mon. Weather Rev., 105(9), 1119–1135, doi:10.1175/1520-0493(1977)105<1119:TSAEOT>2.0.CO;2, 1977.

Fritz, A. and Samenow, J.: Harvey unloaded 33 trillion gallons of water in the {U.S.}, [online] Available from: https://www.washingtonpost.com/news/capital-weather-gang/wp/2017/08/30/harvey-has-unloaded-24-5-trillion-gallons-of-water-on-texas-and-louisiana/?utm_term=.e32e1837ee3d, 2017.

Gray, W. M. and Jacobson Jr., R. W.: Diurnal Variation of Deep Cumulus Convection, Mon. Weather Rev., 105(9), 1171–1188, doi:10.1175/1520-0493(1977)105<1171:DVODCC>2.0.CO;2, 1977.

Hai-Long, S., Qing-Hong, Z. and Bin, X.: Diurnal Variation of Tropical Cyclone Rainfall in the Western North Pacific in 2008--2010, Atmos. Ocean. Sci. Lett., 6(2), 103–108, doi:10.1080/16742834.2013.11447064, 2013.

Hobgood, J. S.: A Possible Mechanism for the Diurnal Oscillations of Tropical Cyclones, J. Atmos. Sci., 43(23), 2901–2922, doi:10.1175/1520-0469(1986)043<2901:APMFTD>2.0.CO;2, 1986.

Hornik, K. and Grün, B.: {movMF}: An {R} Package for Fitting Mixtures of von Mises-

Fisher Distributions, J. Stat. Softw., 58(10), 1–31, doi:10.18637/jss.v058.i10, 2014.

Hou, A. Y., Kakar, R. K., Neeck, S., Azarbarzin, A. A., Kummerow, C. D., Kojima, M., Oki, R., Nakamura, K. and Iguchi, T.: The {G}lobal {P}recipitation {M}easurement Mission, Bull Amer Meteor Soc, 95(5), 701–722, doi:10.1175/BAMS-D-13-00164.1, 2014.

Hu, H., Duan, Y., Wang, Y. and Zhang, X.: Diurnal Cycle of Rainfall Associated with Landfalling Tropical Cyclones in China from Rain Gauge Observations, J. Appl. Meteorol. Climatol., 56(9), 2595–2605, doi:10.1175/JAMC-D-16-0335.1, 2017.

Huffman, G. J., Bolvin, D. T., Nelkin, E. J., Wolff, D. B., Adler, R. F., Gu, G., Hong, Y., Bowman, K. P. and Stocker, E. F.: The {TRMM} {M}ultisatellite {P}recipitation {A}nalysis {(TMPA)}: Quasi-Global, Multiyear, Combined-Sensor Precipitation Estimates at Fine Scales, J Hydrometeor, 8(1), 38–55, doi:10.1175/JHM560.1, 2007.

Huffman, G. J., Bolvin, D. T. and Nelkin, E. J.: {I}ntegrated {M}ulti-satellit{E} {R}etrievals for {GPM (IMERG)} {T}echnical {D}ocumentation., 2017a.

Huffman, G. J., Bolvin, D. T., Braithwaite, D., Hsu, K., Joyce, R., Kidd, C., Nelkin, E. J., Sorooshian, S., Tan, J. and Xie, P.: {NASA} {G}lobal {P}recipitation {M}easurement {I}ntegrated {M}ulti-satellit{E} {R}etrievals for {GPM (IMERG)}. {A}lgorithm {T}heoretical {B}asis {D}ocument, version 4.6, 2017b.

Huffman, G. J., Bolvin, D. T., Nelkin, E. J. and Stocker, E. F.: {V04 IMERG } {F}inal {R}un Release Notes. {NASA} {T}ech. {D}oc., 2017c.

Jiang, H., Halverson, J. B. and Zipser, E. J.: Influence of environmental moisture on {TRMM}-derived tropical cyclone precipitation over land and ocean, Geophys. Res. Lett., 35(17), n/a--n/a, doi:10.1029/2008GL034658, 2008.

Jiang, H., Liu, C. and Zipser, E. J.: A {TRMM-Based} Tropical Cyclone Cloud and Precipitation Feature Database, J. Appl. Meteorol. Climatol., 50(6), 1255–1274, doi:10.1175/2011JAMC2662.1, 2011.

Khouakhi, A., Villarini, G. and Vecchi, G. A.: Contribution of Tropical Cyclones to Rainfall at the Global Scale, J. Clim., 30(1), 359–372, doi:10.1175/JCLI-D-16-0298.1, 2017.

Kirschbaum, D. and Patel, K. G.: Precipitation data key to food security and public health, Eos (Washington. DC)., 97(7), 10 [online] Available from: https://eos.org/meeting-reports/precipitation-data-key-to-food-security-and-public-health, 2016.

Knapp, K. R., Kruk, M. C., Levinson, D. H., Diamond, H. J. and Neumann, C. J.: The {I}nternational {B}est {T}rack {A}rchive for {C}limate {S}tewardship ({IBT}r{ACS}), Bull. Amer. Meteor. Soc., 91(3), 363–376, doi:10.1175/2009BAMS2755.1, 2010.

Kossin, J. P.: Daily Hurricane Variability Inferred from {GOES} Infrared Imagery, Mon. Weather Rev., 130(9), 2260–2270, doi:10.1175/1520-0493(2002)130<2260:DHVIFG>2.0.CO;2, 2002.

Kraus, E. B.: The Diurnal Precipitation Change over the Sea, J. Atmos. Sci., 20(6), 551–556, doi:10.1175/1520-0469(1963)020<0551:TDPCOT>2.0.CO;2, 1963.

Lajoie, F. A. and Butterworth, I. J.: Oscillation of High-Level Cirrus and Heavy Precipitation around Australian Region Tropical Cyclones, Mon. Weather Rev., 112(3), 535–544, doi:10.1175/1520-0493(1984)112<0535:OOHLCA>2.0.CO;2, 1984.

Lark, R. M., Clifford, D. and Waters, C. N.: Modelling complex geological circular data with the projected normal distribution and mixtures of von Mises distributions, Solid Earth, 5(2), 631–639, doi:10.5194/se-5-631-2014, 2014.

Leppert II, K. D. and Cecil, D. J.: Tropical Cyclone Diurnal Cycle as Observed by {TRMM}, Mon. Weather Rev., 144(8), 2793–2808, doi:10.1175/MWR-D-15-0358.1, 2016.

Lonfat, M., Jr., F. D. M. and Chen, S. S.: Precipitation Distribution in Tropical Cyclones Using the Tropical Rainfall Measuring Mission (TRMM) Microwave Imager: A Global Perspective, Mon. Weather Rev., 132(7), 1645–1660, doi:10.1175/1520-0493(2004)132<1645:PDITCU>2.0.CO;2, 2004.

Mardia, K. V: 3 - {B}asic {C}oncepts and {T}heoretical {M}odels, in Statistics of Directional Data, edited by Z. W. Birnbaum and E. Lukas, pp. 39–79, Academic Press., 1972a.

Mardia, K. V: Statistics of Directional Data, 1st ed., edited by Z. W. Birnbaum and E. Lukas, Academic Press, London, Great Britain. [online] Available from: https://www.elsevier.com/books/statistics-of-directional-data/mardia/978-0-12-471150-1, 1972b.

Mardia, K. V and Jupp, P. E.: Directional Statistics, John Wiley \& Sons, Ltd., West Sussex, PO19 1UD England., 2000.

Masseran, N.: Modeling a Multi-modal Distribution of Wind Direction Data in Kudat, Malaysia, Pakistan J. Stat. Oper. Res., 11(2), 195–212, doi:10.18187/pjsor.v11i2.974, 2015.

Melhauser, C. and Zhang, F.: Diurnal Radiation Cycle Impact on the Pregenesis Environment of Hurricane {K}arl (2010), J. Atmos. Sci., 71(4), 1241–1259, doi:10.1175/JAS-D-13-0116.1, 2014.

Mendelsohn, R., Emanuel, K., Chonabayashi, S. and Bakkensen, L.: The impact of climate change on global tropical cyclone damage, Nat. Clim. Chang., 2(3), 205–209, doi:10.1038/nclimate1357, 2012.

Moravec, E. R.: Texas officials: {H}urricane {H}arvey death toll at 82, “mass casualties have absolutely not happened,” [online] Available from: https://www.washingtonpost.com/national/texas-officials-hurricane-harvey-death-toll-at-82-mass-casualties-have-absolutely-not-happened/2017/09/14/bff3ffea-9975-11e7-87fc-c3f7ee4035c9_story.html?utm_term=.d9e372423251, 2017.

Muramatsu, T.: Diurnal Variations of Satellite-Measured {T$_{\text{BB}}$} Areal Distribution and Eye Diameter of Mature Typhoons, J. Meteorol. Soc. Japan. Ser. II, 61(1), 77–90, doi:10.2151/jmsj1965.61.1_77, 1983.

Murray, R. F. and Morgenstern, Y.: Cue combination on the circle and the sphere, J. Vis., 10(11), 1–11, doi:10.1167/10.11.15, 2010.

Navarro, E. L., Hakim, G. J. and Willoughby, H. E.: Balanced Response of an Axisymmetric Tropical Cyclone to Periodic Diurnal Heating, J. Atmos. Sci., 74(10), 3325–3337, doi:10.1175/JAS-D-16-0279.1, 2017.

NOAA-WPC: STORM SUMMARY NUMBER 20 FOR TROPICAL DEPRESSION HARVEY PRELIMINARY RAINFALL TOTALS AND WIND REPORTS, 2017.

O’Neill, M. E., Perez-Betancourt, D. and Wing, A. A.: Accessible Environments for Diurnal-Period Waves in Simulated Tropical Cyclones, J. Atmos. Sci., 74(8), 2489–2502, doi:10.1175/JAS-D-16-0294.1, 2017.

van Oldenborgh, G. J., van der Wiel, K., Sebastian, A., Singh, R., Arrighi, J., Otto, F., Haustein, K., Li, S., Vecchi, G. and Cullen, H.: Attribution of extreme rainfall from Hurricane Harvey, August 2017, Environ. Res. Lett., 12(12), 124009, doi:10.1088/1748-9326/aa9ef2, 2017.

Oliveira, M., Crujeiras, R. M. and Rodríguez-Casal, A.: A plug-in rule for bandwidth selection in circular density estimation, Comput. Stat. \& Data Anal., 56(12), 3898–3908, doi:10.1016/j.csda.2012.05.021, 2012.

Peduzzi, P., Chatenoux, B., Dao, H., De Bono, A., Herold, C., Kossin, J., Mouton, F. and Nordbeck, O.: Global trends in tropical cyclone risk, Nat. Clim. Chang., 2(4), 289–294, doi:10.1038/nclimate1410, 2012.

Pewsey, A., Neuhäuser, M. and D., R. G.: Circular Statistics in {R}, 1st ed., Oxford University Press, Oxford, United Kingdom. [online] Available from: http://circstatinr.st-andrews.ac.uk/index.html, 2013.

Prat, O. P. and Nelson, B. R.: Mapping the world's tropical cyclone rainfall contribution over land using the {TRMM} {M}ulti-satellite {P}recipitation {A}nalysis, Water Resour. Res., 49(11), 7236–7254, doi:10.1002/wrcr.20527, 2013.

Prat, O. P. and Nelson, B. R.: On the Link between Tropical Cyclones and Daily Rainfall Extremes Derived from Global Satellite Observations, J. Clim., 29(17), 6127–6135, doi:10.1175/JCLI-D-16-0289.1, 2016.

Qin, X., Cunningham, P. and Salter-Townshend, M.: Online Trans-dimensional Von Mises-Fisher Mixture Models for User Profiles, J. Mach. Learn. Res., 17(1), 7021–7071 [online] Available from: http://dl.acm.org/citation.cfm?id=2946645.3053482, 2016.

R Core Team: R: A Language and Environment for Statistical Computing, [online] Available from: https://www.r-project.org/, 2017.

Rios Gaona, M. F., Villarini, G., Zhang, W. and Vecchi, G. A.: The added value of {IMERG} in characterizing rainfall in tropical cyclones, Atmos. Res., 209, 95--102, doi:10.1016/j.atmosres.2018.03.008, 2018.

Risser, M. D. and Wehner, M. F.: Attributable human-induced changes in the likelihood and magnitude of the observed extreme precipitation during Hurricane Harvey, Geophys. Res. Lett., n/a--n/a, doi:10.1002/2017GL075888, 2017.

Samenow, J.: Nearly 65 inches of rain fell from {H}urricane {H}arvey in {T}exas, shattering {U.S.} storm record, [online] Available from: https://www.washingtonpost.com/news/capital-weather-gang/wp/2017/08/29/harvey-marks-the-most-extreme-rain-event-in-u-s-history/?utm_term=.1c10e1f2ef49, 2017.

Schneider, U., Becker, A., Finger, P., Meyer-Christoffer, A., Rudolf, B. and Ziese, M.: {GPCC} {F}ull {D}ata {R}eanalysis {V}ersion 7.0 at 0.5°: Monthly Land-Surface Precipitation from Rain-Gauges built on {GTS}-based and Historic Data, , doi:10.5676/DWD_GPCC/FD_M_V7_050, 2015a.

Schneider, U., Becker, A., Finger, P., Meyer-Christoffer, A. and Ziese, M.: {GPCC} {M}onitoring {P}roduct: Near Real-Time Monthly Land-Surface Precipitation from Rain-Gauges based on {SYNOP} and {CLIMAT} data, , doi:10.5676/DWD_GPCC/MP_M_V5_100, 2015b.

Serra, Y. L. and McPhaden, M. J.: In Situ Observations of Diurnal Variability in Rainfall over the Tropical Pacific and Atlantic Oceans, J. Clim., 17(18), 3496–3509, doi:10.1175/1520-0442(2004)017<3496:ISOODV>2.0.CO;2, 2004.

Simpson, R. H.: The Hurricane Disaster-Potential Scale, Weatherwise, 27(4), 169–186, doi:10.1080/00431672.1974.9931702, 1974.

Stanley, T., Kirschbaum, D. B., Huffman, G. J. and Adler, R. F.: Approximating Long-Term Statistics Early in the {G}lobal {P}recipitation {M}easurement Era, Earth Interact, 21(3), 1–10, doi:10.1175/EI-D-16-0025.1, 2017.

Sundqvist, H.: Numerical simulation of the development of tropical cyclones with a ten-level model. Part II, Tellus, 22(5), 504–510, doi:10.1111/j.2153-3490.1970.tb00516.x, 1970.

Tang, X. and Zhang, F.: Impacts of the Diurnal Radiation Cycle on the Formation, Intensity, and Structure of Hurricane Edouard (2014), J. Atmos. Sci., 73(7), 2871–2892, doi:10.1175/JAS-D-15-0283.1, 2016.

Tang, X., Tan, Z.-M., Fang, J., Sun, Y. Q. and Zhang, F.: Impact of the Diurnal Radiation Cycle on Secondary Eyewall Formation, J. Atmos. Sci., 74(9), 3079–3098, doi:10.1175/JAS-D-17-0020.1, 2017.

Tsagris, M., Athineou, G. and Sajib, A.: Directional: Directional Statistics, [online] Available from: https://cran.r-project.org/package=Directional, 2017.

Tuleya, R. E. and Kurihara, Y.: A Numerical Study on the Effects of Environmental Flow on Tropical Storm Genesis, Mon. Weather Rev., 109(12), 2487–2506, doi:10.1175/1520-0493(1981)109<2487:ANSOTE>2.0.CO;2, 1981.

UNDP: Reducing disaster risk: A challenge for development, [online] Available from: http://www.undp.org/content/dam/undp/library/crisis%5C prevention/disaster/asia_pacific/Reducing%5C Disaster%5C risk%5C a%5C Challenge%5C for%5C development.pdf, 2004.

UNISDR and CRED: The human cost of weather-related disasters 1995-2015, [online] Available from: https://www.unisdr.org/2015/docs/climatechange/COP21_WeatherDisastersReport_2015_FINAL.pdf, 2017.

Villarini, G.: On the seasonality of flooding across the continental United States, Adv. Water Resour., 87, 80–91, doi:10.1016/j.advwatres.2015.11.009, 2016.

Wu, Q., Ruan, Z., Chen, D. and Lian, T.: Diurnal variations of tropical cyclone precipitation in the inner and outer rainbands, J. Geophys. Res. Atmos., 120(1), 1–11, doi:10.1002/2014JD022190, 2015.